ASTRONOMY & ASTROPHYSICS
SUPPLEMENT SERIES

Astron. Astrophys. Suppl. Ser. **143**, 391–403 (2000)

ROSAT HRI catalogue of X-ray sources in the LMC region*

M. Sasaki, F. Haberl, and W. Pietsch

Max–Planck–Institut für extraterrestrische Physik, Giessenbachstraße, D-85748 Garching, Germany

Received December 30, 1999; accepted January 20, 2000

Abstract. All 543 pointed observations of the ROSAT High Resolution Imager (HRI) with exposure times higher than 50 s and performed between 1990 and 1998 in a field of $10° \times 10°$ covering the Large Magellanic Cloud (LMC) were analyzed. A catalogue was produced containing 397 X-ray sources with their properties measured by the HRI. The list was cross-correlated with the ROSAT Position Sensitive Propotional Counter (PSPC) source catalogue presented by Haberl & Pietsch (1999) in order to obtain the hardness ratios for the X-ray sources detected by both instruments. 138 HRI sources are contained in the PSPC catalogue, 259 sources are new detections. The spatial resolution of the HRI was higher than that of the PSPC and the source position could be determined with errors mostly smaller than 15″ which are dominated by systematic attitude errors. After cross-correlating the source catalogue with the SIMBAD data base and the TYCHO catalogue 94 HRI sources were identified with known objects based on their positional coincidence and X-ray properties. Whenever more accurate coordinates were given in catalogues or literature for identified sources, the X-ray coordinates were corrected and the systematic error of the X-ray position was reduced. For other sources observed simultaneously with an identified source the coordinates were improved as well. In total the X-ray position of 254 sources could be newly determined. The catalogue contains 39 foreground stars, 24 supernova remnants (SNRs), five supersoft sources (SSSs), nine X-ray binaries (XBs), and nine AGN well known from literature. Another eight sources were identified with known candidates for these source classes. Additional 21 HRI sources are suggested in the present work as candidates for SNR, X-ray binary in the LMC, or background AGN because of their extent, hardness ratios, X-ray to optical flux ratio, or flux variability.

Key words: catalogues — galaxies: Magellanic Clouds — galaxies: stellar content — X-rays: galaxies — X-rays: stars

1. Introduction

The Magellanic Clouds (MCs) as the nearest galaxies to the Milky Way allow us to resolve their stellar content in various wavelength bands. X-ray observations combined with optical and radio data can be used to investigate the physical properties of individual X-ray sources as well as the statistical properties of different source classes in a galaxy as a whole. The quantitative and positional distribution of X-ray sources in the MCs will help us to understand the unresolved X-ray emission from more distant galaxies.

After the first observation of X-ray emission from the MCs in 1968 (Mark et al. 1969) four permanent (LMC X–1, X–2, X–3, and X–4, Leong et al. 1971; Giacconi et al. 1972) and few transient X-ray sources were found in the LMC in several satellite missions (UHURU, SAS-3, Copernicus, Ariel-V, HEAO-1). An extensive pointed survey of the LMC was performed by the Einstein Observatory between 1979 and 1981. The two detectors on board this satellite, the Imaging Proportional Counter and the High Resolution Imager, were sensitive enough to detect X-ray binaries, SSSs, and SNRs at the distance of the LMC (55 kpc). Long et al. (1981) published a list of 97 discrete X-ray sources in the direction of the LMC and the same data was re-analyzed by Wang et al. (1991) finally giving a list of 105 sources. 54 discrete X-ray sources were identified with objects in the LMC, most of the remaining sources were associated with foreground stars and background AGN. In EXOSAT observations few

Send offprint requests to: M. Sasaki,
e-mail: manami@mpe.mpg.de

* Table 4 is only and Tables 1–3 are also available in electronic form at the CDS via anonymous ftp to cdsarc.u-strasbg.fr (130.79.128.5) or via http://cdsweb.u-strasbg.fr/Abstract.html

additional X-ray sources were found (Jones et al. 1985; Pakull et al. 1985; Pietsch et al. 1989).

The next thorough survey of the LMC was made by ROSAT in the energy range of 0.1 − 2.4 keV (Trümper 1982). From 1990 to 1998 ROSAT performed more than 700 pointed observations in a 10 by 10 degree field centered on the LMC. Haberl & Pietsch (1999b, hereafter HP99b) analyzed 212 PSPC observations and created a catalogue of 758 X-ray sources.

In this work results of the analysis of the ROSAT HRI data of the LMC are presented. A description of the HRI detector can be found in David et al. (1996). A source catalogue was obtained in a similar way as in HP99b and many sources were identified by cross-correlating the source list with other existing catalogues. With the help of known properties of different source classes we looked for new candidates for SNRs, stars, and hard X-ray sources which mainly consist of X-ray binaries and absorbed background AGN.

2. ROSAT HRI data

2.1. Data analysis

The LMC was observed by the ROSAT HRI in more than 500 pointings during the operational phase of ROSAT between 1990 and 1998. 543 observations with exposure times of 50 to 110000 s (Fig. 1) in a field of $10° \times 10°$ around RA = $05^{\rm h}\ 25^{\rm m}\ 00^{\rm s}$, Dec = $-67°\ 43'\ 20''$ (J2000.0) were used for the analysis. The analysis was carried out using three detection methods available in EXSAS (Zimmermann et al. 1994). For each pointing X-ray sources were searched using the sliding window methods with local background and with a spline fitted background map. The resulting detection lists were merged and a maximum likelihood algorithm was performed on this list. Sources were accepted if their likelihood of existence was larger than 10.0, i.e. the existence probability was higher than $P = 1 - \exp(-ML_{\rm exi}) = 1 - 4.5\ 10^{-5}$, and their telescope off-axis angle smaller than $15'$ during the observation.

For point and point like sources the source extent was determined by the maximum likelihood technique fitting the source intensity distribution with a Gaussian profile. The count rates resulting from this calculation are correct only for sources with small extent and a brightness profile peaking in the center. For extended sources like SNRs with ringlike structure the net count rates were determined interactively by integrating the counts within a circle around the source. For the background the counts were averaged in a ring around the source distant enough not to be influenced by the source emission.

In order to increase the sensitivity HRI observations with pointing directions within a radius of $1'$ were merged after adjusting their position. This was possible for 56 different regions in the LMC. Source detection was also performed on these data and additional faint sources were found which were not detectable in single pointings.

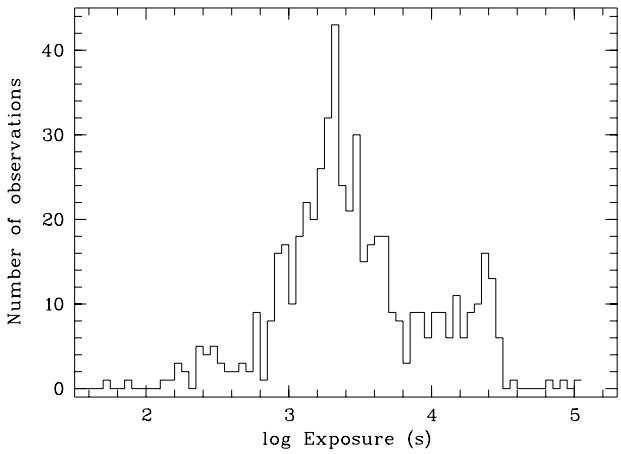

Fig. 1. Histogram of HRI pointing exposure times

The final source lists obtained for each pointing and co-added observations were merged to one list and multiple detections of a source were reduced to one detection for each source. For this purpose the detection with the smallest positional error was chosen. After screening manually in order to delete spurious detections like knots in extended emission, the catalogue finally contains 397 distinct sources.

2.2. Positional corrections and error

ROSAT observations suffer from a systematic positional uncertainty of about $7''$ (Kürster 1993). For minimizing this systematic error the coordinates of identified objects were compared to high accuracy positions available in the TYCHO catalogue obtained from the ESA Hipparcos space astrometry satellite (Hoeg et al. 1997) or in the literature. First the X-ray position was corrected to TYCHO coordinates. For sources without any TYCHO counterpart, but identified on the ESO Digitized Sky Survey (DSS) frame with other stars on this frame which were listed in the TYCHO catalogue, more accurate coordinates were calculated for HRI sources by determining the offset between the TYCHO and DSS positions and between the HRI and DSS position. Other sources could be identified with objects in the SIMBAD data base operated at the Centre de Données astronomiques de Strasbourg or in the literature and their positions were corrected after checking their positions on DSS frames. Correction of coordinates for one source implied improved coordinates for all detections of this source in different pointings and for other sources in same pointings. Those secondary corrections again allowed correction of further pointings if the sources were detected several times. Finally for 254 out of 397 sources improved coordinates were determined.

In cases where positional correction was possible the remaining systematic error consists of the error in

former optical measurements and the statistical error of the identified source. For not corrected sources the systematic error was set to $7''$. The positional error was finally computed as a composite of the statistical uncertainty with 90% confidence and the systematic error. It is used throughout the paper for the error circle. After the source detection procedure the mean positional error was $8\farcs3$. The coordinate correction reduced the mean positional error of all sources to $6\farcs4$. For position corrected sources the mean positional error is $5\farcs1$.

2.3. Correlation with existing catalogues

The catalogue was cross-correlated with the SIMBAD data base and the TYCHO catalogue in order to identify HRI sources. The HRI catalogue contains samples of known SSSs, X-ray binaries, SNRs, Galactic foreground stars, and background AGN. The catalogue was also cross-correlated with the source list from the pointed PSPC observations (HP99b). 138 HRI sources are identical with sources which were detected in PSPC data and thus for most of them the hardness ratios (HR1, HR2) are known. Since the HRI had no spectral resolution no information on the X-ray spectrum could be obtained for HRI sources which are completely new detections. A total of 94 HRI sources were identified with known objects like SSSs, X-ray binaries, SNRs, stars, and background AGN.

With the help of their X-ray properties like extent, extent likelihood, PSPC hardness ratios, X-ray to optical flux ratio (see Sect. 3.2), and X-ray variability 14 previously unknown HRI sources and 7 sources also listed in the PSPC catalogue were newly classified.

The whole source catalogue from HRI observations with the corrected coordinates, final positional error, existence likelihood, HRI count rate, extent, extent likelihood, PSPC count rate and the corresponding PSPC source number with hardness ratios (HP99b) is given in Table 4. For each HRI and PSPC count rate the results for the pointing with the smallest positional error, determined by the maximum likelihood algorithm, were selected. Therefore HRI count rates in the table are representative for one single observation for each source. For extended SNRs the given count rate may correspond to a knot within the source. PSPC count rates are taken from the PSPC catalogue (HP99b) if available. For HRI sources without PSPC detection we derived 2σ upper limit from the pointing with the highest exposure time. If the source was too close to the rim or the window support structure of the PSPC detector, no count rate is given in Table 4. Neither was it possible to determine PSPC count rates or upper limits for sources located in regions with diffuse emission.

2.4. Flux variability

About 80% of HRI sources were observed more than once and allow time variability studies. For point and point like sources longterm lightcurves were produced with observation-average count rates or upper limits determined by the maximum likelihood algorithm, whereas for extended sources integrated count rates within a circle were used (see Sect. 2.1). For some very bright sources the count rates were integrated in the same way, because an apparent extent resulted from the maximum likelihood algorithm. An apparent extent is computed if the high photon statistics of the bright sources cause a significant deviation from the assumed model for the point spread function.

A χ^2-test for a constant count rate was performed and the factor between the maximum and minimum flux was computed for each lightcurve. Together with the reduced χ^2 this flux factor was used to characterize variability on long time scales of days to years (see also HP99a). For SNRs we expect constant integrated flux, however the flux factor was in the range of 1.0 to 1.8. This may be caused by different off-axis angles and/or different extraction of the extended source. Therefore variations below a factor of 2.0 should be handled with care as they might indicate no real variability but false integration of the source flux because of the extent or existence of a nearby bright source.

In order to obtain a complete lightcurve of the ROSAT observations, also PSPC count rates and upper limits were calculated for the HRI sources. In Figs. 2a–c the PSPC to HRI count rate conversion factor is plotted over $N_{\rm H} = 10^{20} - 10^{23}$ cm^{-2} for three different spectral models. SSSs with a soft black body spectrum can be modeled with $T = 10.0 - 50.0$ eV and galactic $N_{\rm H} = 10^{20} - 10^{21}$ cm^{-2} in the direction of the LMC. XBs in general show a power law spectrum with $N_{\rm H}$ up to 10^{22} cm^{-2} because of intrinsic absorption $N_{\rm H}$. So for most of the point and point like X-ray sources PSPC count rates can be converted into HRI count rates by dividing by a typical value of 3, though for very soft sources this scale factor can be larger. Sources in regions with extended emission (e.g. 30 Dor or N44) or close to another source can not always be resolved in PSPC data and may result in false large converting factor.

χ^2 and the flux factor were again calculated for all lightcurves including PSPC count rates (divided by 3.0) and upper limits. Finally 26 sources show significant variability with reduced $\chi^2 > 5$ corresponding to a probability > 0.9999 (see Table 1). Four of them are new classified HRI sources (for sources Nos. 49 and 364 see Sect. 3.2.4, for Nos. 300 and 313 see Sect. 3.2.2). As example the lightcurve of source No. 49, a new HRI candidate for a variable X-ray binary or AGN is shown in Fig. 3.

PSPC count rates were determined in as many pointings as possible. The mean value was calculated from these count rates and compared to the HRI mean count rates (see Fig. 4). The resulting conversion factor is close to 3.0, only variable sources marked with dots show bigger deviation.

Table 1. HRI sources with significant flux variability

1	2	3	4	5	6	7	8
No	Rate HRI [cts s^{-1}]	Rate PSPC [cts s^{-1}]	$\frac{F_{max}}{F_{min}}$	Red. χ^2	DOF	No PSPC	Remarks
19	*4.6e-1	*2.3e-3	598.1	376.1	1	331	HMXB RX J0502.9–6626 (CAL E)
20	5.3e-2	7.7e-2	4.5	163.5	2	380	AGN RX J0503.1–6634, $z = 0.064$ [SCF94]
23	2.4e-2	2.1e-2	3.4	61.9	1	715	
49	*4.9e-3	*7.5e-3	4.3	9.4	4	559	<XB> or <AGN>
65	2.2e-3	1.9	25611.5	663.9	45	1030	SSS RX J0513.9–6951
103	4.1e-3	2.8e-3	10.5	10.2	6		foreground star HD 35862
124	1.8e-2	1.0e-1	4.9	19.6	20	1094	AGN RX J0524.0–7011, $z = 0.151$ [SCF94]
155	*8.3e-3	*4.2e-3	132.1	18.7	30		Nova LMC 1995 [OG99]
167	1.4e-3	1.2e-1	256.1	51.6	26	1039	SSS RX J0527.8–6954
180	*1.9	*7.5	11.2	691.6	74	122	foreground star K1III& HD 36705 (AB Dor)
193	3.4e-2	1.7e-1	2.6	7.0	8	749	foreground star G5 HD 269620 [CSM97]
202	2.0e-3	8.5e-2	1022.5	11.9	20	204	HMXB Be/X RXJ0529.8–6556 [HDP97]
218	8.4e-3	3.7e-1	344.9	99.9	10	252	HMXB Be/X EXO053109-6609 [HDP95a], [DHP96]
233	6.0e-3	2.2e-2	66.1	7.9	13	184	HMXB RX J0532.5–6551 (Sk–65 66) [HPD95b]
239	*8.9e-2	*4.9	367.1	10247.6	25	316	HMXB LMC X–4, HD 269743 O8III
293	4.4e-2	1.6e-1	2.1	9.4	18	902	foreground star dMe CAL 69 [CSM97]
300	5.4e-3		18.9	414.6	2		<stellar>, source not resolved by the PSPC
306	*6.0	*23.4	2.5	1838.8	22	41	HMXB LMC X–3
311	3.5	13.5	1.6	576.1	29	1001	HMXB LMC X–1, O8III
313	*6.3e-3	*8.3e-3	3.7	9.3	3	668	<stellar>
348	4.3e-2		284.0	775.9	6	654	SSS CAL 83 [SCF94], one PSPC point., source near rim
349	3.0e-2	1.0e-1	19.5	7.2	5	61	foreground star? [HP99a]
352	1.3e-3	1.2e-2	3.1	10.0	2	1225	HMXB RX J0544.1–7100 [HP99b]
363	6.1e-2	1.3e-1	1.5	36.8	3	1240	SSS CAL 87
364	1.2e-2		30.5	158.4	1	747	<XB> or <AGN>, one PSPC pointing, source near rib
375	3.3e-3	3.3e-2	4.5	6.1	4	1127	foreground star F3/F5IV/V HD 39756

Notes to columns 2 and 3: For point and point like sources count rates are the mean of output values from maximum likelihood algorithm for single pointings. For extended sources and bright sources with apparent extent (see text) the average of integrated count rates in single pointings was taken (* in front of the number).

Notes to column 6: Degrees of freedom.

Notes to column 7: Source number from HP99b.

Notes to column 8: Sources classified in this work are put in < >. Abbreviations for references in square brackets are given in literature list.

3. Source classes

In Sect. 3.1 we discuss HRI sources which were identified either with sources already known from literature or with candidates which were found in former X-ray studies and in PSPC data (HP99b). Section 3.2 deals with new classification of HRI sources based on their X-ray properties.

3.1. Source identification

For 97 HRI sources out of 138 which were also detected by the PSPC the HRI observation yielded smaller positional error circles and consequently more accurate source positions compared to the PSPC results. Therefore for several sources likely optical counterparts could be determined which was not possible only with PSPC data.

94 HRI sources were identified with known objects in the LMC, foreground stars, or background objects mainly based on their position (see Sect. 2.3). As they comprise different source types X-ray properties characteristic for each source class could be derived from HRI and PSPC data. Table 2 lists HRI sources with identification.

HP99b have shown that extent and extent likelihood as well as the hardness ratios measured by the PSPC have characteristic values for different source classes and can be used as classification criteria.

In Fig. 5 extent and extent likelihood of the HRI sources are shown. The extent was calculated in the maximum likelihood algorithm and so gives the value resulting from fitting Gaussians. Thus in some cases it may not be the extent of the whole source but only of knots which were found within the extended source. Identified

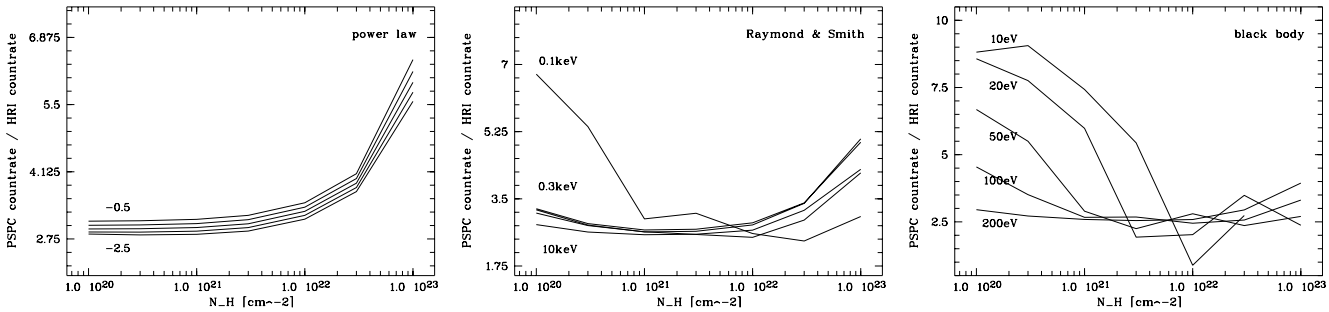

a. power law spectra with photon index: –2.5, –2.0, –1.5, –1.0, –0.5

b. Raymond & Smith spectra with T = 0.1, 0.3, 1.0, 3.0, 10.0 keV

c. black body spectra with T = 10.0 – 200.0 eV

Fig. 2. PSPC/HRI conversion factor as function of $N_{\rm H}$ for power law, Raymond & Smith, and black body spectra

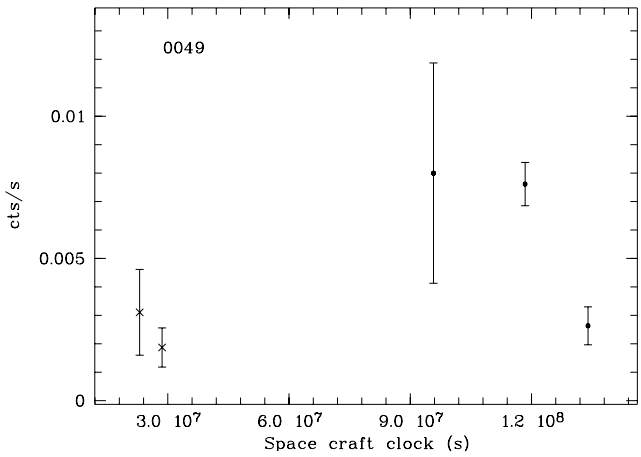

Fig. 3. Lightcurve of source No. 49. Crosses for converted PSPC count rates, dots for HRI count rates. Zero point of the space craft clock is 1990, June 21 21:06:50 UT

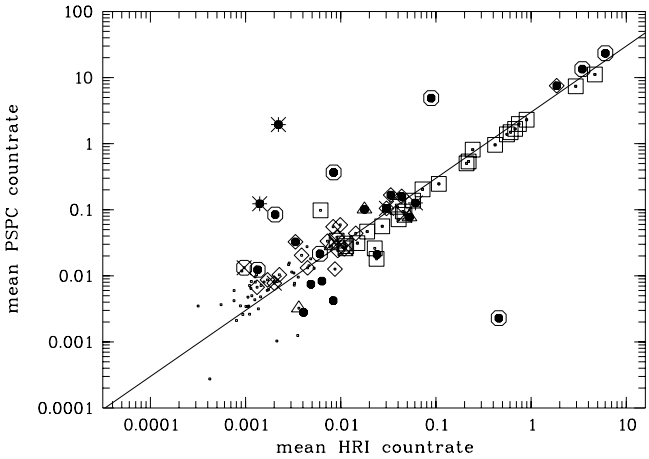

Fig. 4. Mean of observation-averaged count rates from PSPC pointings over mean of observation-averaged count rates from HRI pointings for ROSAT sources. Squares indicate SNRs, lozenges stars, hexagons XBs, triangles AGN, and asterisks SSSs. Crossed symbols are already known candidates. Variable sources are additionally marked with filled dots. The line indicates a PSPC/HRI conversion factor of 3

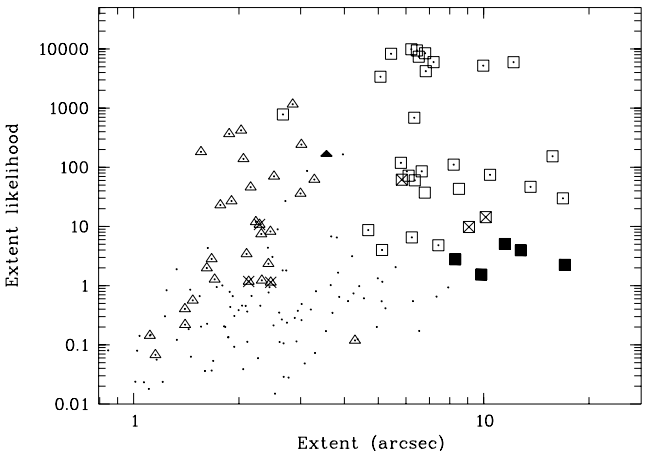

Fig. 5. Source extent and extent likelihood of HRI sources in the LMC. SNRs are marked with open squares, known point sources with open triangles. Crossed symbols are candidates for SNRs or point sources known from literature, filled symbols are new classifications

SNRs, marked with open squares, are distributed in the region with large extent and high extent likelihood. Crossed squares indicate known SNR candidates and filled squares sources newly classified as SNR candidates in this work. Point sources have lower extent likelihood unless they were extremely bright like AB Dor (No. 180), LMC X–1 (No. 311), or RX J0439.8–6809 (No. 4) where the deviation of the point spread function from the assumed Gaussian profile becomes significant.

3.1.1. Foreground stars

By cross-correlating the HRI source catalogue with SIMBAD and TYCHO catalogues and using the finding charts presented by Schmidtke et al. (1994, hereafter SCF94), Cowley at al. (1997, hereafter CSM97), and Schmidtke et al. (1999, hereafter SCC99) 39 sources were identified with Galactic foreground stars (Table 2). Most of them could also be identified with the help of *UBV* photometry results presented by Gochermann et al. (1993) and Grothues et al. (1997). On DSS-images there

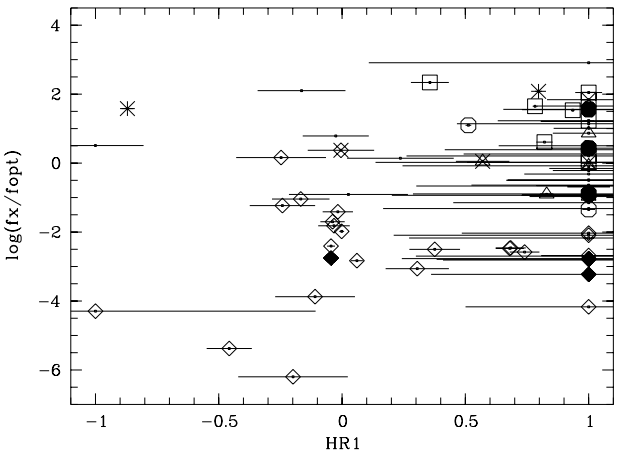

Fig. 6. Flux ratio $\log(f_x/f_{opt})$ as a function of hardness ratio 1. Open squares are SNRs, open lozenges stars, open hexagons XBs, open triangles AGN, and asterisks SSSs. Crossed symbols are already known candidates and filled symbols are new classifications

are point sources as very likely optical counterparts at the positions of these HRI sources within the error circle.

Based on hardness ratios of the PSPC observations two point sources were suggested as foreground star candidates by HP99b (Nos. 189 and 349). They were detected in PSPC images and their hardness ratios are within the range characteristic of stars (HP99b). DSS images show an optical point source within the improved HRI error circle in both cases.

3.1.2. Supernova remnants

Most SNRs in the LMC are extended X-ray sources which could be resolved by the HRI. They typically show extents of about $5'' - 20''$ and high extent likelihood (> 10.0). A total of 24 known SNRs were observed by the HRI, four HRI sources are identified with known SNR candidates (Nos. 50, 231, 310, and 315). For both Nos. 231 and 310 the measured hardness ratios are typical for SNRs. No. 50 has a harder X-ray spectrum with HR1 $= 1.00 \pm 0.10$ and HR2 $= 0.34 \pm 0.07$.

3.1.3. Supersoft sources

SSSs have very soft X-ray spectra and so far seven SSSs have been discovered in the LMC (HP99b). Two of them were sources of the Einstein LMC survey (Long et al. 1981) and five were found with the help of the ROSAT PSPC. In the HRI pointings five LMC SSSs listed in Table 2 were observed and detected with high existence likelihood.

3.1.4. X-ray binaries

Characteristic for most X-ray binaries is the hard X-ray spectrum and flux variability. In HRI observations nine bright sources could be identified with well known massive X-ray binaries (HMXB). The point source RX J0532.7–6926, here No. 238, has been suggested to be a low mass X-ray binary (LMXB) candidate by Haberl & Pietsch (1999a, hereafter HP99a) and was also detected by the HRI. In HP99a a lightcurve with PSPC and HRI measurements is presented and variability is discussed in detail. Between 1990 and 1993 the source showed an exponential intensity decay.

3.1.5. AGN

Nine known background AGN with redshifts between 0.06 and 0.44 (SCF94; CSM97; Crampton et al. 1997) were re-identified in the HRI pointings. Because of its positional coincidence with the radio source PKS 0552–640 and its hardness ratios measured by the PSPC the HRI source No. 389 was classified as AGN candidate (No. 37 in HP99b). On the DSS frame an optical source with $m_B = 16.3$ within the HRI error circle is identified as the most likely optical counterpart.

3.2. New classifications

The extensive detection list produced from the HRI pointings towards the LMC allowed us to search for new candidates for different source types. In the course of studying the newly discovered HRI sources the following parameters were of prime importance: count rates, source extent, extent likelihood, flux variability, and counterparts in other wavelengths.

In addition to these X-ray properties we calculated the X-ray to optical flux ratio of HRI sources, for which possible optical counterparts could be found. The flux ratio was computed according to the equation $\log(f_x/f_{opt}) = \log(3 \cdot \text{HRI counts/s} \cdot 10^{-11}) + 0.4\, m_B + 5.37$ (Maccacaro et al. 1988; HP99b). The relation used for PSPC observations in HP99b was applied here for HRI sources converting the HRI count rates to PSPC count rates by multiplying by the factor of 3 which is typical for hard sources. B magnitudes from the USNO-A1.0 Catalogue produced by the United States Naval Observatory (Monet 1996) were used. For several sources the optical counterpart could not be determined uniquely. In such a case the magnitude of the brightest optical object within the error circle was used resulting in lower limits for $\log(f_x/f_{opt})$. For the SNRs $\log(f_x/f_{opt})$ in general gives no quantitative information, but is an indicator that this source class is bright in X-ray ($\log(f_x/f_{opt}) > -1$).

As one can see in Fig. 6 stars in general have negative $\log(f_x/f_{opt})$, for AGN it is around zero, and for SSSs and XBs it is mostly positive in particular when they were observed in their X-ray active phase. Combination of f_x/f_{opt} and the hardness ratios provides a tool to exclude foreground stars.

Newly discovered HRI sources which are suggested as candidates for different source classes in this work can be found in Table 3 and are discussed in the following.

Table 2. Identified HRI sources in the LMC

1	2	3	4	5	6	7	8	9	10	11	12
No	RA (J2000.0)	Dec	r_{90} [″]	$ML_{\rm exi}$	Count rate [cts s^{-1}]	$r_{\rm ext}$ [″]	$ML_{\rm ext}$	No PSPC	HR1	HR2	Remarks
9	04 53 43.5	−68 24 23	4.4	15.3	5.99e-04 ± 1.63e-04	1.2 ± 1.9	0.1				foreground star G0 HD 268717 [GGO93]
12	04 54 30.2	−68 18 01	9.1	12.7	1.30e-03 ± 3.20e-04	0.0 ± 0.0	0.0				foreground star HD 31961
15	04 58 25.1	−69 08 22	4.1	39.8	5.77e-03 ± 1.31e-03	2.3 ± 2.0	1.2	816	1.00 ± 0.51	0.29 ± 0.13	foreground star F7V [CSM97]
16	04 58 43.9	−68 50 50	4.1	317.5	4.48e-02 ± 3.74e-03	0.0 ± 0.0	0.0	742	−0.04 ± 0.05	0.09 ± 0.07	foreground star dMe HD 268840 [CSM97]
18	05 02 09.3	−66 20 36	5.3	16.2	7.81e-03 ± 3.22e-03	0.4 ± 2.7	0.0	304	0.68 ± 0.06	0.08 ± 0.08	foreground star K0III [SCF94]
24	05 05 27.1	−67 43 14	7.1	425.8	1.48e-02 ± 1.10e-03	0.0 ± 0.0	0.0	568	0.74 ± 0.06	0.18 ± 0.09	foreground eclipsing binary star ASAS J050526–6743.2
63	05 13 39.4	−69 32 00	6.5	33.1	6.14e-03 ± 1.40e-03	0.0 ± 0.0	0.0	943			foreground star K1V [CSM97]
71	05 14 26.8	−69 57 05	1.7	160.7	3.52e-03 ± 3.08e-04	1.7 ± 1.4	1.3				foreground star HD 269255
79	05 16 07.2	−68 15 35	2.4	691.7	7.17e-02 ± 4.31e-03	0.0 ± 0.0	0.0	636	−0.03 ± 0.06	−0.09 ± 0.09	foreground star G1V [SCF94]
87	05 17 25.8	−71 31 58	15.1	17.3	7.26e-03 ± 1.82e-03	4.3 ± 6.2	0.1	1284	1.00 ± 0.79	−0.09 ± 0.10	foreground star K2III& HD 35324
91	05 18 32.3	−68 13 33	1.7	201.4	1.47e-02 ± 1.85e-03	1.7 ± 1.2	2.8	634	−1.00 ± 1.37		foreground star K3V HD 269320 [GGO93], [SCF94]
99	05 19 56.2	−71 29 07	6.3	25.8	8.53e-03 ± 2.61e-03	0.4 ± 2.7	0.0	1280	0.30 ± 0.13	0.35 ± 0.10	foreground star K2III [SCF94]
103	05 22 08.2	−68 04 28	2.4	124.0	5.61e-03 ± 5.50e-04	0.0 ± 0.0	0.0				foreground star HD 35862
104	05 22 19.6	−67 51 31	2.7	30.5	1.72e-03 ± 3.14e-04	1.4 ± 1.5	0.4				foreground star HD 269422
117	05 23 13.3	−69 33 43	3.7	39.8	9.61e-04 ± 1.36e-04	0.9 ± 3.2	0.0	954	1.00 ± 0.50		foreground star GSC 09166–00446
123	05 24 01.4	−71 09 33	7.1	455.0	5.64e-02 ± 5.15e-03	3.0 ± 1.3	36.1	1242	−0.17 ± 0.12	0.24 ± 0.19	foreground star M5e 1E 0524.7–7112
133	05 25 02.3	−67 53 28	8.7	27.0	4.48e-03 ± 9.35e-04	0.0 ± 0.0	0.0	595	0.38 ± 0.10	0.08 ± 0.12	foreground star K2IV, RS CVn? [CSM97]
140	05 25 38.4	−69 35 43	0.6	1847.2	7.64e-03 ± 2.55e-04	2.5 ± 0.8	70.3	964	0.30 ± 0.08	−0.01 ± 0.10	foreground star F7V HD 36436 [CSM97]
145	05 25 58.1	−70 11 07	2.1	259.6	7.57e-03 ± 6.45e-04	0.0 ± 0.0	0.0	1093	0.68 ± 0.06	0.23 ± 0.07	foreground star K2IV–V, RS CVn [SCF94]
154	05 26 34.9	−63 41 34	3.5	21.5	8.72e-04 ± 2.44e-04	0.0 ± 0.0	0.0				foreground star HD 36355
156	05 26 59.8	−68 37 22	3.8	45.0	2.37e-03 ± 3.87e-04	0.0 ± 0.0	0.0	693	−0.46 ± 0.09	−0.47 ± 0.16	foreground star F0IV–V HD 36584
171	05 28 11.7	−71 05 38	8.1	19.0	1.39e-03 ± 2.79e-04	0.0 ± 0.0	0.0				foreground star F3/F5V HD 36877
176	05 28 26.8	−70 54 02	8.3	24.1	2.81e-03 ± 5.26e-04	0.0 ± 0.0	0.0				foreground star G0V HD 36890
178	05 28 32.5	−68 36 13	1.5	734.8	1.18e-02 ± 7.34e-04	2.2 ± 1.1	12.0	687	1.00 ± 0.19	0.01 ± 0.05	foreground star G1V [CSM97]
180	05 28 44.7	−65 26 56	0.2	31209.6	2.36e+00 ± 2.90e-02	2.0 ± 0.4	421.5	122	−0.00 ± 0.01	0.07 ± 0.01	foreground star K1III& HD 36705 (AB Dor)
189	05 29 24.0	−68 49 12	2.3	54.3	1.89e-03 ± 3.18e-04	2.1 ± 1.9	1.2	728	0.23 ± 0.14	0.02 ± 0.17	foreground star? [HP99b]
193	05 29 27.0	−68 52 05	0.6	2800.3	3.33e-02 ± 1.21e-03	1.9 ± 0.8	26.9	749	0.06 ± 0.02	0.04 ± 0.03	foreground star G5 HD 269620 [CSM97]
212	05 30 49.6	−67 05 55	10.0	20.9	1.18e-02 ± 3.76e-03	0.0 ± 0.0	0.0	478	−0.25 ± 0.18	0.34 ± 0.28	foreground star dMe [SCF94]
216	05 31 03.1	−71 06 10	3.5	25.4	9.92e-04 ± 2.34e-04	1.4 ± 1.8	0.2				foreground star GSC 09166-00859
262	05 35 22.8	−66 12 55	8.3	48.9	1.00e-02 ± 1.88e-03	0.0 ± 0.0	0.0	268	−0.24 ± 0.13	−1.00 ± 1.65	foreground star dM4e [CCH84]
293	05 38 15.9	−69 23 30	0.9	2548.9	4.30e-02 ± 1.46e-03	0.6 ± 1.1	0.0	902	0.02 ± 0.03	−0.00 ± 0.04	foreground star dMe CAL 69 [CSM97]
294	05 38 21.3	−68 50 34	2.6	33.2	1.37e-03 ± 2.89e-04	0.0 ± 0.0	0.0				foreground star G5V HD 269916
296	05 38 34.4	−68 53 07	0.4	5091.1	5.56e-02 ± 1.64e-03	0.0 ± 0.0	0.0	752	−0.04 ± 0.02	0.05 ± 0.02	foreground star G2V, RS CVn? [CSM97]
305	05 38 50.0	−69 44 27	4.1	36.0	1.46e-03 ± 2.48e-04	0.0 ± 0.0	0.0				foreground star F2V HD 38329
308	05 39 29.2	−69 57 09	4.4	20.3	8.84e-04 ± 2.24e-04	0.0 ± 0.0	0.0				foreground star HD 269934
349	05 43 34.5	−64 22 55	7.2	624.1	3.06e-02 ± 1.79e-03	0.0 ± 0.0	0.0	61	−0.00 ± 0.13	0.05 ± 0.19	foreground star? [HP99b]
356	05 44 46.4	−65 44 07	3.9	15.3	1.43e-03 ± 5.16e-04	0.0 ± 0.0	0.0	157	−0.20 ± 0.22	−1.00 ± 0.63	foreground star A7V HD 39014
375	05 48 19.2	−70 20 44	1.7	216.6	3.57e-03 ± 3.47e-04	2.3 ± 1.3	7.5	1127			foreground star F3/F5IV/V HD 39756
379	05 49 28.9	−69 47 14	9.9	24.2	1.81e-03 ± 3.34e-04	0.0 ± 0.0	0.0	1014	−1.00 ± 0.89		foreground star F2V HD 39904
383	05 49 46.5	−71 49 36	7.1	570.5	9.56e-03 ± 5.97e-04	3.3 ± 1.2	62.1	1312	−0.02 ± 0.06	−0.16 ± 0.08	foreground star dMe [SCC99]
386	05 51 00.5	−69 54 08	4.4	106.0	1.20e-02 ± 1.73e-03	0.6 ± 3.0	0.0	1036	−0.11 ± 0.16	−1.00 ± 3.23	foreground star F5V HD 40156

Notes to column 9 (Table 2), 10 (Tables 3 and 4):Catalogue number from [HP99b].
Notes to column 12 (Table 2), 13 (Tables 3 and 4):
fg: foreground.
Candidates from literature are marked with ? behind the source class.
New classification of this work are put in < >.
Abbreviations for references in square brackets are given in the literature list.

Table 2. continued

1	2	3	4	5	6	7	8	9	10	11	12
No	RA (J2000.0)	Dec	r_{90} [″]	$ML_{\rm exi}$	Count rate [cts s^{-1}]	$r_{\rm ext}$ [″]	$ML_{\rm ext}$	No PSPC	HR1	HR2	Remarks
8	04 53 38.0	−68 29 20	3.2	392.8	1.66e-02 ± 7.28e-04	6.3 ± 1.4	687.9	670	0.86 ± 0.01	−0.36 ± 0.01	SNR 0453–68.5
13	04 54 47.3	−66 25 44	8.3	96.2	8.53e-03 ± 7.03e-04	13.6 ± 4.5	46.7	329	0.84 ± 0.04	−0.24 ± 0.05	SNR LHA 120–N 11L
25	05 05 42.0	−67 52 29	7.0	2223.3	5.83e-02 ± 1.40e-03	6.8 ± 1.1	4214.3	592	0.81 ± 0.01	−0.21 ± 0.01	SNR DEM L 71
27	05 05 55.5	−68 01 51	7.0	7040.7	2.16e-01 ± 3.25e-03	12.2 ± 1.7	5968.8	614	0.89 ± 0.01	−0.19 ± 0.02	SNR LHA 120–N 23
43	05 08 58.6	−68 43 35	7.0	13431.0	5.04e-01 ± 7.44e-03	5.4 ± 0.8	8288.7	707	0.97 ± 0.00	0.13 ± 0.01	SNR LHA 120–N 103B
47	05 09 31.3	−67 31 17	7.0	5476.1	6.33e-02 ± 1.11e-03	6.5 ± 0.9	7396.2	542	0.78 ± 0.01	−0.27 ± 0.01	SNR 0509.0–67.5
50	05 10 48.7	−68 45 27	7.6	21.3	4.16e-03 ± 1.28e-03	0.0 ± 0.0	0.4	712	1.00 ± 0.10	0.34 ± 0.07	SNR? [WHHW91]
97	05 19 34.3	−69 02 01	7.0	8929.9	2.58e-01 ± 3.80e-03	6.2 ± 0.8	9883.6	789	0.95 ± 0.00	−0.02 ± 0.01	SNR 0519–69.0
98	05 19 48.9	−69 26 09	7.9	45.9	8.54e-03 ± 8.38e-04	10.4 ± 3.5	74.6	915	0.36 ± 0.08	−0.14 ± 0.10	SNR 0520–69.4
114	05 23 02.4	−67 53 00	4.9	17.4	3.13e-03 ± 5.53e-04	6.2 ± 2.8	6.5	594	1.00 ± 0.04	0.17 ± 0.06	SNR 0523–67.9 [CMG93]
132	05 25 01.9	−69 38 51	0.5	7939.5	2.66e-01 ± 2.44e-03	6.4 ± 0.9	9439.5	977	0.94 ± 0.00	−0.04 ± 0.01	SNR LHA 120–N 132D
136	05 25 22.9	−65 59 17	7.0	2178.7	4.85e-02 ± 5.97e-04	10.0 ± 1.4	5218.8	219	0.94 ± 0.01	−0.14 ± 0.02	SNR LHA 120–N 49B
146	05 26 00.1	−66 05 19	7.0	5983.6	7.83e-02 ± 5.44e-04	6.8 ± 0.9	8459.6	241	0.95 ± 0.00	−0.02 ± 0.01	SNR LHA 120–N 49
166	05 27 45.6	−69 11 51	7.9	23.4	1.74e-03 ± 3.23e-04	4.7 ± 2.5	8.7	836	1.00 ± 0.74	1.00 ± 6.84	SNR 0528–69.2
223	05 31 56.7	−70 59 59	3.4	71.6	4.76e-03 ± 3.79e-04	8.2 ± 2.5	110.9	1222	1.00 ± 0.09	−0.26 ± 0.04	SNR LHA 120–N 206
231	05 32 27.3	−67 31 10	8.5	106.1	1.80e-02 ± 1.99e-03	9.1 ± 4.8	9.8	540	1.00 ± 0.49	−0.45 ± 0.09	SNR? 0532–67.5 [C97]
248	05 33 55.7	−69 54 47	8.1	102.9	4.42e-02 ± 3.39e-03	15.7 ± 4.7	153.6	1043	1.00 ± 0.11	−0.20 ± 0.05	SNR 0534–69.9
252	05 34 16.3	−70 33 43	10.6	10.5	3.99e-03 ± 1.08e-03	7.4 ± 4.5	4.8	1160	0.82 ± 0.03	0.08 ± 0.04	SNR DEM L 238
268	05 35 45.7	−69 18 00	1.5	63.8	1.36e-03 ± 9.48e-05	5.8 ± 1.6	119.1	866	1.00 ± 0.09	−0.14 ± 0.05	SNR Honeycomb Nebula
269	05 35 46.5	−66 02 23	7.0	3681.1	3.11e-01 ± 6.77e-03	7.2 ± 1.1	5993.1	226	0.94 ± 0.00	−0.01 ± 0.01	SNR LHA 120–N 63A
270	05 35 48.9	−69 09 31	2.8	47.9	9.83e-04 ± 9.34e-05	6.8 ± 2.4	37.3				SNR 0536-69.2, 30 DOR C: knot
274	05 36 06.6	−70 38 57	9.2	11.0	3.46e-03 ± 1.06e-03	5.1 ± 3.5	4.0	1173	1.00 ± 0.02	−0.17 ± 0.04	SNR DEM L 249
276	05 36 17.3	−69 13 04	2.0	55.0	1.14e-03 ± 9.25e-05	6.1 ± 1.9	72.0	840	0.89 ± *	0.11 ± *	SNR 0536–69.2, 30 DOR C: knot
277	05 36 19.0	−69 09 30	3.2	64.0	1.37e-03 ± 1.15e-04	8.5 ± 2.7	43.2				SNR 0536-69.2, 30 DOR C: knot
289	05 37 46.9	−69 10 18	0.4	8036.1	4.07e-02 ± 6.36e-04	5.1 ± 0.7	3391.0	826	1.00 ± 0.02	0.47 ± 0.02	SNR 0538–69.1, LHA 120–N 157B (CAL 67)
310	05 39 36.6	−70 01 58	9.3	27.1	4.28e-03 ± 6.40e-04	10.1 ± 4.4	14.4	1063	1.00 ± 0.17	−0.17 ± 0.10	SNR? [HP99b]
315	05 40 04.5	−69 43 58	3.6	41.3	3.36e-03 ± 3.52e-04	5.8 ± 2.0	61.8				SNR? [CKS97]
318	05 40 10.9	−69 19 52	0.7	17883.4	1.95e-01 ± 3.32e-03	2.7 ± 0.5	781.3	877	0.98 ± 0.00	0.58 ± 0.01	SNR LHA 120–N 158A, PSR B0540–69
365	05 46 57.1	−69 42 40	10.7	32.2	7.62e-03 ± 8.64e-04	16.8 ± 6.2	29.9	993	0.95 ± *	0.21 ± *	SNR LHA 120–N 135, shell B
366	05 47 18.5	−69 41 28	7.4	29.7	3.41e-03 ± 3.51e-04	6.7 ± 2.2	85.5	987	1.00 ± 0.10	0.22 ± 0.07	SNR LHA 120–N 135, shell A
372	05 47 47.6	−70 24 46	3.0	37.3	8.31e-03 ± 1.11e-03	6.4 ± 2.5	60.3	1137	1.00 ± 0.05	−0.10 ± 0.06	SNR 0548–70.4
4	04 39 49.6	−68 09 01	0.4	6228.5	1.66e-01 ± 4.89e-03	2.1 ± 0.6	138.9	628	−1.00 ± 0.01		SSS RX J0439.8–6809
65	05 13 50.7	−69 51 46	1.2	16279.1	3.09e-01 ± 2.41e-03	2.8 ± 0.5	1161.2	1030	−0.86 ± 0.00	−0.98 ± 0.01	SSS RX J0513.9–6951
167	05 27 49.4	−69 54 05	4.3	21.1	5.08e-04 ± 1.24e-04	0.0 ± 0.0	0.0	1039	−1.00 ± 0.01		SSS RX J0527.8–6954
348	05 43 34.2	−68 22 21	1.1	17776.1	2.15e-01 ± 3.26e-03	2.2 ± 0.7	46.1	654	−0.87 ± 0.02	−1.00 ± 0.51	SSS CAL 83 [SCF94]
363	05 46 46.9	−71 08 52	7.0	3268.5	6.23e-02 ± 2.17e-03	3.0 ± 0.8	242.1	1240	0.80 ± 0.01	−0.86 ± 0.01	SSS CAL 87
17	05 01 23.9	−70 33 33	2.9	58.0	1.12e-02 ± 2.64e-03	1.1 ± 1.5	0.1				HMXB RX J0501.6–7034 (CAL 9)
19	05 02 51.6	−66 26 25	1.2	2361.6	4.35e-01 ± 2.26e-02	1.8 ± 0.8	23.0	331	1.00 ± 0.67	0.43 ± 0.18	HMXB RX J0502.9–6626 (CAL E)
202	05 29 48.3	−65 56 46	2.0	119.2	1.94e-03 ± 2.05e-04	0.0 ± 0.0	0.0	204	0.84 ± 0.04	0.49 ± 0.06	HMXB Be/X transient RXJ0529.8–6556
218	05 31 13.5	−66 07 09	0.8	1133.4	9.42e-03 ± 4.08e-04	0.0 ± 0.0	0.0	252	0.64 ± 0.03	0.27 ± 0.04	HMXB Be/X transient EXO053109–6609
233	05 32 33.1	−65 51 43	1.4	327.0	3.99e-03 ± 2.80e-04	0.0 ± 0.0	0.0	184	1.00 ± 0.10	0.43 ± 0.05	HMXB RX J0532.5–6551
238	05 32 42.8	−69 26 18	3.9	29.3	1.35e-03 ± 2.82e-04	2.5 ± 2.1	1.1	914	1.00 ± 0.31	0.29 ± 0.19	LMXB? RX J0532.7–6926 [HP99a]
239	05 32 49.5	−66 22 13	0.2	30957.4	2.82e+00 ± 4.22e-02	1.6 ± 0.4	182.5	316	0.51 ± 0.01	0.12 ± 0.02	HMXB LMC X–4, HD 269743 O8III
306	05 38 56.3	−64 05 03	0.2	34020.7	7.37e+00 ± 6.88e-02	1.9 ± 0.4	367.4	41	0.84 ± 0.00	0.28 ± 0.01	HMXB LMC X–3
311	05 39 38.7	−69 44 32	3.0	32679.3	3.77e+00 ± 4.68e-02	0.0 ± 0.0	0.0	1001	0.99 ± 0.00	0.74 ± 0.00	HMXB LMC X–1, O8III
352	05 44 06.0	−71 00 51	7.8	12.3	1.34e-03 ± 5.17e-04	0.0 ± 0.0	0.0	1225	1.00 ± 0.03	0.65 ± 0.03	HMXB RX J0544.1–7100 [HP99b]

Table 2. continued

1	2	3	4	5	6	7	8	9	10	11	12
No	RA (J2000.0)	Dec	r_{90} [″]	$ML_{\rm exi}$	Count rate [cts s^{-1}]	$r_{\rm ext}$ [″]	$ML_{\rm ext}$	No PSPC	HR1	HR2	Remarks
10	04 54 10.7	−66 43 17	7.3	55.1	8.01e-03 ± 1.82e-03	1.5 ± 1.5	0.6	411	1.00 ± 0.24	0.29 ± 0.07	AGN RX J0454.2–6643, $z = 0.228$ [CGC97]
20	05 03 04.0	−66 33 44	2.2	188.8	5.35e-02 ± 8.03e-03	0.0 ± 0.0	0.0	380	0.83 ± 0.03	0.17 ± 0.03	AGN RX J0503.1–6634, $z = 0.064$ [SCF94]
86	05 17 16.9	−70 44 01	2.2	186.4	1.03e-02 ± 1.24e-03	2.5 ± 1.4	8.2				AGN RX J0517.3–7044, z=0.169 [CSM97]
124	05 24 02.5	−70 11 09	1.6	800.1	1.57e-02 ± 8.88e-04	1.6 ± 1.2	2.0	1094	0.91 ± 0.02	0.27 ± 0.04	AGN RX J0524.0–7011, $z = 0.151$ [SCF94]
220	05 31 31.8	−71 29 46	3.5	46.4	1.19e-02 ± 3.54e-03	0.0 ± 0.0	0.0				AGN RX J0531.5–7130, z=0.221 [SCF94]
224	05 31 59.9	−69 19 51	3.5	46.4	2.81e-03 ± 5.53e-04	2.4 ± 1.9	2.3	876	1.00 ± 0.21	0.02 ± 0.09	AGN RX J0532.0–6920, $z = 0.149$ [SCF94]
257	05 34 44.6	−67 38 56	8.5	41.1	6.03e-03 ± 1.13e-03	0.0 ± 0.0	0.0	561	1.00 ± 0.15	−0.04 ± 0.15	AGN RX J0534.8–6739, $z = 0.072$ [CSM97]
371	05 47 45.2	−67 45 05	2.6	89.0	9.63e-03 ± 1.75e-03	2.1 ± 1.5	3.4				AGN RX J0547.8–6745, z=0.391 [CSM97]
385	05 50 31.5	−71 09 57	8.6	29.1	3.59e-03 ± 7.58e-04	0.5 ± 3.7	0.0	1243	1.00 ± 0.75	1.00 ± 1.61	AGN RX J0550.5–7110, $z = 0.443$ [CGC97]
389	05 52 24.3	−64 02 12	7.1	464.0	4.82e-02 ± 4.64e-03	2.3 ± 1.2	10.8	37	0.57 ± 0.11	0.17 ± 0.12	AGN? PKS 0552–640 [HP99b]

Table 3. Classified HRI sources

1	2	3	4	5	6	7	8	9	10	11	12	13
No	RA (J2000.0)	Dec	r_{90} [″]	$ML_{\rm exi}$	Count rate [cts s^{-1}]	$r_{\rm ext}$ [″]	$ML_{\rm ext}$	$\log(f_{\rm x}/f_{\rm opt})$	No PSPC	HR1	HR2	Remarks
28	05 05 58.4	−68 10 30	8.4	22.8	1.85e-03 ± 4.21e-04	2.7 ± 3.4	0.2	−3.09				<stellar>
29	05 06 16.7	−68 15 09	9.7	30.5	3.82e-03 ± 6.81e-04	0.0 ± 0.0	0.0	−2.77				<stellar>
49	05 10 28.7	−67 37 41	7.1	484.0	5.01e-03 ± 3.10e-04	0.0 ± 0.0	0.0	−0.89	559	1.00 ± 0.71	0.26 ± 0.16	<XB> or <AGN>
90	05 17 47.8	−71 44 05	11.4	15.9	1.96e-03 ± 6.46e-04	1.9 ± 2.3	0.3	−3.06	1305	1.00 ± 1.34	0.45 ± 0.15	<stellar>
135	05 25 22.5	−69 49 16	4.9	29.6	2.12e-03 ± 3.86e-04	0.0 ± 0.0	0.0	−3.23	1025	1.00 ± 0.64	1.00 ± 2.40	<stellar>
197	05 29 39.2	−66 08 06	20.1	12.7	1.96e-03 ± 4.05e-04	17.1 ± 10.8	2.2	−0.62				<SNR>
217	05 31 13.1	−68 25 48	7.7	21.8	1.09e-03 ± 2.78e-04	0.0 ± 0.0	0.0	−3.11	661		1.00 ± 1.10	<stellar>
229	05 32 15.6	−71 04 26	4.8	14.1	8.18e-04 ± 2.30e-04	0.0 ± 0.0	0.0	−3.48				<stellar>
230	05 32 18.5	−71 07 43	2.9	302.5	4.69e-03 ± 3.49e-04	0.0 ± 0.0	0.0	1.56	1238	1.00 ± 0.35	1.00 ± 0.98	<XB> or <AGN>
254	05 34 27.7	−69 25 40	5.9	11.0	2.65e-03 ± 9.41e-04	0.0 ± 0.0	0.0	−2.77				<stellar>
284	05 37 28.6	−69 23 18	13.4	11.5	4.07e-03 ± 1.05e-03	9.8 ± 7.6	1.5	−1.58				<SNR>
287	05 37 35.9	−68 25 57	7.4	115.8	3.15e-03 ± 3.26e-04	0.0 ± 0.0	0.0	−3.34				<stellar>
288	05 37 36.2	−69 16 42	9.7	16.3	8.36e-04 ± 1.40e-04	11.5 ± 5.5	5.1	−0.51				<SNR>
300	05 38 42.4	−68 52 41	1.5	103.8	2.75e-03 ± 3.86e-04	0.8 ± 1.3	0.1	−2.75				<stellar>
307	05 39 27.9	−69 33 12	12.0	15.7	2.49e-03 ± 4.68e-04	12.8 ± 6.5	4.0	0.76				<SNR>
313	05 39 59.9	−68 28 42	7.1	315.3	6.31e-03 ± 5.22e-04	2.7 ± 1.2	26.9	−2.79	668	1.00 ± 0.62	1.00 ± 1.88	<stellar>
328	05 41 22.2	−69 36 29	6.6	11.1	7.28e-04 ± 2.03e-04	0.0 ± 0.0	0.0	−0.77				<HMXB> LMC B2 supergiant star
332	05 41 37.1	−68 32 32	4.5	33.6	2.34e-03 ± 4.27e-04	0.0 ± 0.0	0.0	−2.34				<HMXB> LMC O star
338	05 42 01.2	−69 24 44	11.9	11.5	2.43e-03 ± 5.91e-04	8.3 ± 5.6	2.8	0.47				<SNR>
347	05 43 22.2	−68 56 39	6.4	141.3	2.51e-03 ± 3.01e-04	1.2 ± 1.1	0.8	−3.07				<stellar>
364	05 46 55.7	−68 51 35	7.0	1146.0	2.02e-02 ± 1.00e-03	3.6 ± 1.0	171.7	0.43	747	1.00 ± 0.21	1.00 ± 0.60	<XB> or <AGN>

3.2.1. SNR candidates

Investigating the extent five HRI sources (Nos. 197, 284, 288, 307, 338) not classified with the help of PSPC observations are suggested as SNR candidates as their extent is larger than 8″ (see Fig. 5). Since they were not detected by the PSPC because of short exposure times there is no spectral information about these sources which might be crucial for further improvement of the classification.

3.2.2. Sources classified as stellar

For 11 HRI sources probable optical counterparts were found within the error circle which are all bright ($m_B \leq 12.5$), and their $\log(f_x/f_{opt})$ is negative (< -2.0). For this reason these sources are classified as stellar objects, and in particular the brightest objects are likely foreground stars. Four sources were also observed by the PSPC (Nos. 90, 135, 217, 313), but as the errors of their hardness ratios are large, no spectral information is given.

The lightcurve of No. 300 shows a strong decrease of the X-ray emission with a factor of 10 in 2 years indicating that the HRI observations were performed after an emission maximum. The point source in the optical DSS image at the HRI position is very likely the optical counterpart with a B magnitude of $m_B = 12.4$ according to the USNO–A1.0 Catalogue and $\log(f_x/f_{opt}) = -2.75$.

3.2.3. LMC stars as candidates for high mass X-ray binaries

Two X-ray point sources detected by the HRI were identified with known LMC O and B stars (No. 328, Sanduleak 1970, $m_B = 18.8$ and No. 332, Brunet et al. 1975, $m_B = 13.6$) because of the positional coincidence. With HRI data no variability investigations could be carried out for these X-ray sources, though there exist many pointings in their direction, because they were both detected only once and in other pointings the upper limits were too high for this purpose. But their identification with optically selected LMC stars allows us to classify them as candidates for high mass X-ray binaries.

3.2.4. Sources with hard X-ray spectrum: Candidates for AGN or X-ray binary

With the help of the hardness ratios and other characteristics measured by the HRI like flux variability or f_x/f_{opt} three HRI sources which were also detected by the PSPC could be classified as candidates either for X-ray binary or for AGN.

The point source No. 49 shows significant flux variations, as it is shown in Fig. 3, and has a hard and/or highly absorbed X-ray spectrum (HR1 = 1.00 ± 0.71, HR2 = 0.26 ± 0.16). On the DSS image a likely optical counterpart with a B magnitude of 16.4 (according to the USNO–A1.0 Catalogue) is found. Therefore this source has been classified as a candidate either for an X-ray binary or AGN.

Sources Nos. 230 and 364 are further candidates for X-ray binary or AGN as they have a hard and/or absorbed X-ray spectrum (HR1 = 1.00 ± 0.35, HR2 = 1.00 ± 0.98 and HR1 = 1.00 ± 0.21, HR2 = 1.00 ± 0.60 respectively). Since source No. 230 has a small positional error a probable optical counterpart can be found on the DSS image. This counterpart is faint ($m_B = 22.6$), and we obtain a high $\log(f_x/f_{opt})$ of 1.56. For source No. 364 there is a relatively faint optical source ($m_B = 18.2$) within the error circle which might be the counterpart ($\log(f_x/f_{opt}) = 0.43$).

Another nine sources detected by the HRI were identified with sources in the PSPC catalogue (HP99b) showing a hard X-ray spectrum. But from the HRI observations no additional information could be obtained. Thus the HRI sources are simply classified as hard X-ray sources because of the hardness ratios of their PSPC detections.

3.3. Source distribution

Due to the high spatial resolution of the HRI many sources could be detected both in the outer regions and in the optical bar region of the LMC. In Fig. 7 HRI sources identified with known objects and known candidates are plotted on a grey scale PSPC image (0.1 − 2.4 keV) of the LMC (from HP99b). The sources are located in different regions of the LMC and show no spatial preferences, it is not only background AGN or foreground stars and candidates which are distributed over the whole LMC region. There are still more than 250 non-identified point sources which are homogeneously distributed in all LMC regions which were covered by ROSAT HRI pointings as it is shown in Fig. 8. In contrast, in PSPC observations not many additional sources could be detected in the regions with strong diffuse emission, because the lower spatial resolution hindered in distinguishing between extended and point like emission (HP99b).

The HRI allows to study the extent of the sources to scales of arcseconds. Therefore SNR candidates could be found not only in regions without surrounding diffuse emission. Four out of five newly suggested SNR candidates are located in regions with diffuse emission between 30 Dor and LMC X-1 (see Fig. 8).

Within and around the optical bar region several new stellar sources and candidates for X-ray binary or AGN were found.

4. Summary

The analysis of all 543 ROSAT HRI pointed observations performed between 1990 and 1998 with exposure times higher than 50 s is presented. Using a maximum likelihood algorithm the source detection resulted in a catalogue of 397 sources which was cross-correlated with the SIMBAD

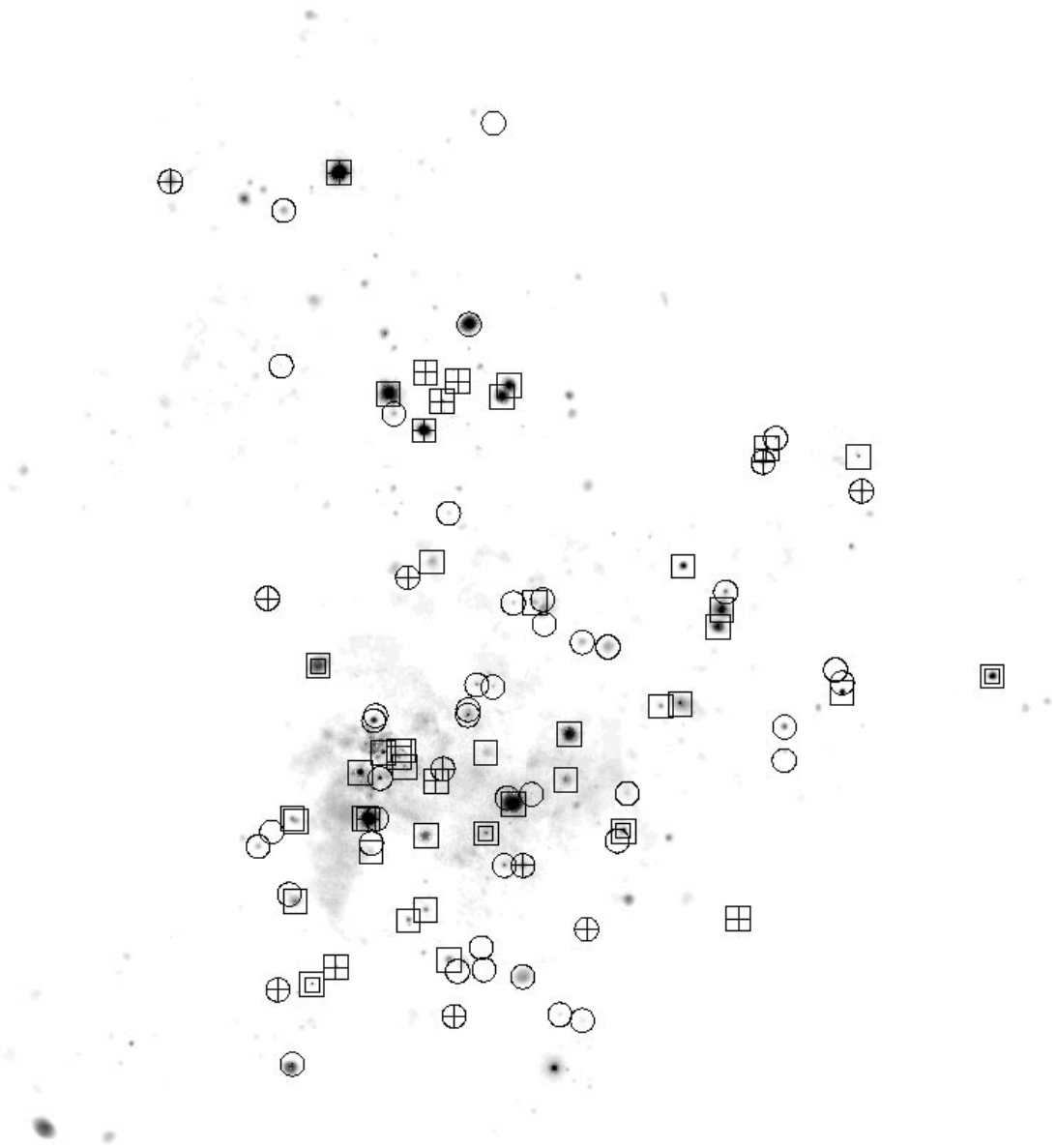

Fig. 7. Identified HRI sources are plotted on a grey scale PSPC image (0.1 − 2.4 keV) of the LMC. Squares are SNRs, circles are foreground stars, double squares SSSs, crossed squares XBs, crossed circles AGN. Candidates from literature are included for each source class

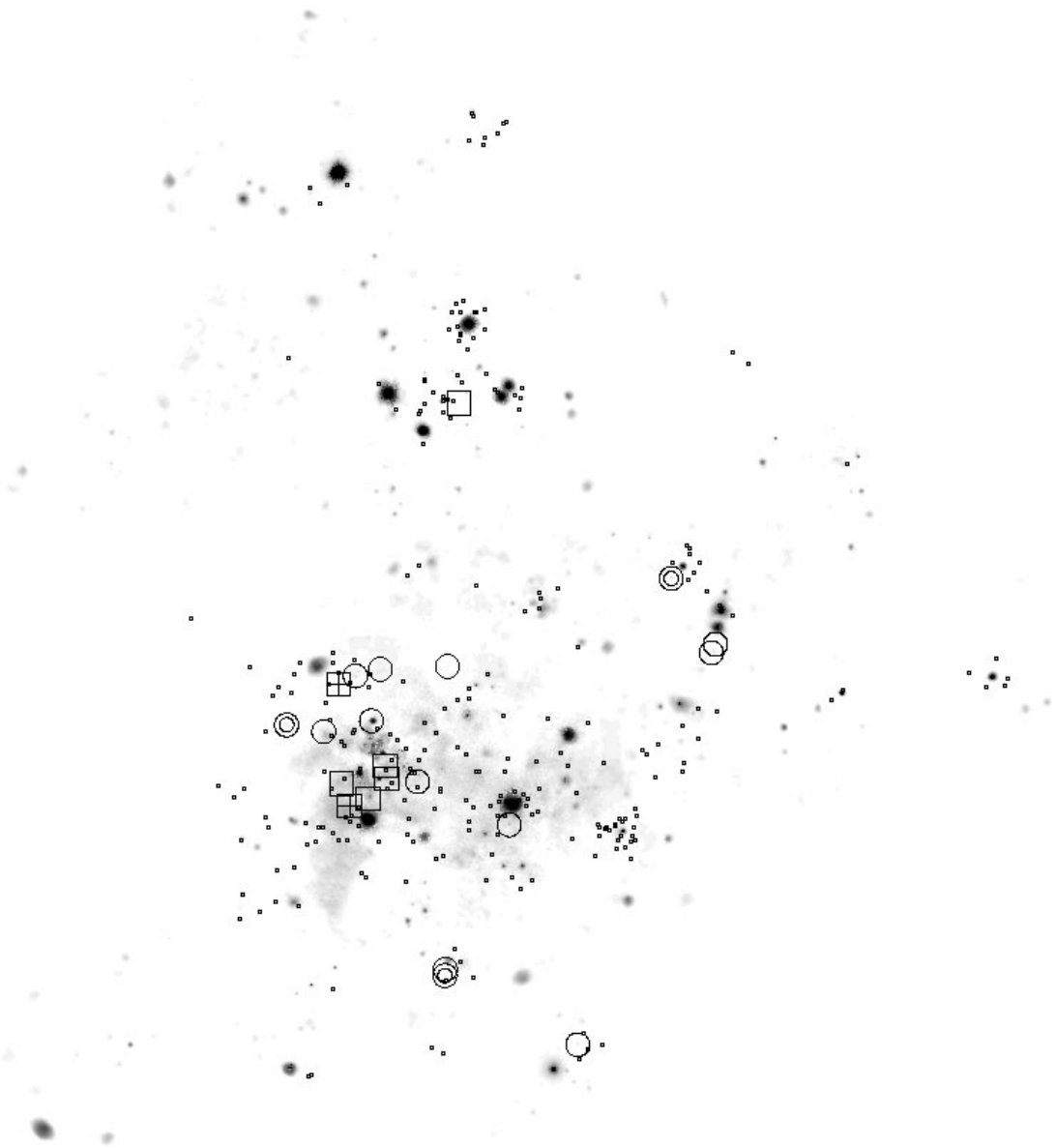

Fig. 8. The distribution of unidentified HRI sources and new source classifications is shown. Unidentified HRI sources are plotted as dots, squares are sources classified as SNR candidates, circles as stellar sources, crossed squares as XB candidates and double circles as candidates for XB or AGN

data base and the TYCHO catalogue. Further X-ray properties could be obtained for HRI sources contained in the PSPC catalogue of HP99b.

The high spatial resolution of the HRI enabled the identification of 94 HRI sources with well known objects based on the positional coincidence and considering their extent and hardness ratios. The coordinates of most of the identified sources could be improved to more accurate positions and allowed the positional correction of other HRI sources. Thus for 254 sources the systematic error for their coordinates could be reduced to values smaller than $7''$ which is the standard systematic error of ROSAT observations.

For different source classes like SSS, X-ray binary, SNR, Galactic stars, and background AGN classification criteria could be derived from the extent and hardness ratios of the identified sources. We looked for flux variability of the sources and for likely optical counterparts. Five newly detected HRI sources were classified as candidates for SNRs because of their extent, two HRI sources which were identified with an LMC O and a B star as HMXB candidates. Eleven sources with probable bright optical counterpart and small X-ray to optical flux ratio are classified as stellar sources. Three sources with hard and/or absorbed X-ray spectrum indicated by the PSPC hardness ratios are likely candidates for X-ray binaries or AGN. Two of the hard X-ray sources show flux variability and for each of these an optical counterpart was found.

With the help of HRI observations many new X-ray sources were found. Further follow-up observations in X-ray, optical, or radio wavelengths with spectral information are needed to characterize these sources in more detail.

Acknowledgements. The ROSAT project is supported by the German Bundesministerium für Bildung und Forschung (BMBF) and the Max-Planck-Gesellschaft. This research has been carried out by making extensive use of the SIMBAD data base operated at CDS, Strasbourg, France.

References

Brunet J.P., Imbert M., Martin N., et al., 1975, A&AS 21, 109
Chu Y.-H., 1997, AJ 113, 1815 [C97]
Chu Y.-H., Kennicutt R.C., Snowden S.L., et al., 1997, PASP 109, 554 [CKS97]
Cowley A.P., Crampton D., Hutchings J.B., et al., 1984, ApJ 286, 196 [CCH84]
Cowley A.P., Schmidtke P.C., McGrath T.K., Ponder A.L., Fertig R.M., 1997, PASP 109, 21 [CSM97]
Crampton D., Gussie G., Cowley A.P., Schmidtke P.C., 1997, AJ 114, 2353 [CGC97]
David L.P., Harnden Jr. F.R., Kearns K.E., Zombeck M.V., 1996, The ROSAT High Resolution Imager (HRI), USRSDC/SAO Calibration Report 1996 February (revised)
Dennerl K., Haberl F., Pietsch W., 1996, in: Zimmermann H.U., Trümper J., Yorke H. (eds.) Proceedings of "Röntgenstrahlung from the Universe", Sept. 25-29 1995, MPE report 263, 131 [DHP96]
Giacconi R., Murray S., Gursky H., et al., 1972, ApJ 178, 281
Gochermann J., Grothues H.-G., Östreicher M.O., Berghöfer T., Schmidt-Kaler T., 1993, A&AS 99, 591 [GGO93]
Grothues H.-G., Östreicher M.O., Gochermann J., Tappert C., Zaum A., Brugger H.R., Schmidt-Kaler T., 1997, A&AS 121, 247 [GOG97]
Haberl F., Dennerl K., Pietsch W., 1995, A&A 302, L1 [HDP95a]
Haberl F., Pietsch W., Dennerl K., 1995, A&A 303, L49 [HPD95b]
Haberl F., Dennerl K., Pietsch W., 1997, A&A 318, 490 [HDP97]
Haberl F., Pietsch W., 1999a, A&A 344, 521 [HP99a]
Haberl F., Pietsch W., 1999b, A&AS 139, 277 [HP99b]
Hoeg E., Bässgen G., Bastian U., et al., 1997, A&A 323, L57
Jones L.R., Pye J.P., McHardy I.M., Fairall A.P., 1985, Space Sci. Rev. 40, 693
Kürster M., 1993, ROSAT Status Report No. 67
Leong C., Kellogg E., Gursky H., Tananbaum H., Giacconi R., 1971, ApJ 170, L67
Long K.S., Helfand D.J., Grabelsky D.A., 1981, ApJ 248, 925
Maccacaro T., Gioia I.M., Wolter A., Zamorani G., Stocke J.T., 1988, ApJ 326, 680
Mark H., Price R., Rodrigues R., Seward F.D., Swift C.D., 1969, ApJ 155, L143
Monet D., 1996, Am. Astron. Soc. Meet. 188, 54.04
Morgan D.H., 1994, A&AS 102, 235 [M94b]
Orio M., Greiner J., 1999, A&A 344, L13 [OG99]
Pakull M., Brunner H., Staubert A., Pietsch W., Beuermann K., 1985, Space Sci. Rev. 40, 379
Pietsch W., Dennerl K., Rosso C., 1989, Proc. 23rd ESLAB Symp. on Two Topics in X-ray Astronomy, Bologna ESA SP-296, p. 573
Sanduleak N., 1970, Contr. Cerro-Tololo Obs., 89
Schmidtke P.C., Cowley A.P., Frattare L.M., et al., 1994, PASP 106, 843 [SCF94]
Schmidtke P.C., Cowley A.P., Crane J.D., Taylor V.A., McGrath T.K., 1999, AJ 117, 927 [SCC99]
Trümper J., 1982, Adv. Space Res. 2, 241
Wang Q., Hamilton T., Helfand D.J., Wu X., 1991, ApJ 374, 475 [WHHW91]
Zimmermann H.U., Becker W., Belloni T., et al., 1994, EXSAS User's Guide, MPE report 257